International Journal of Drug Design and Discovery

***Volume* 4 • *Issue* 2 • *April – June* 2013. 1106-1115**

Comfa Study of A Series of N_1-(Substituted)Aryl-2-(Substituted)-5,7-Dimethyl-pyrido[2,3-D]Pyrimidin-4(3*h*)-One – Histamine H_1-Receptor Antagonists

Bhumika D. Patel[1*], Manjunath D. Ghate[1], Nirzari Gupta[1], Mahesh T. Chhabria[2]

[1]*Department of Pharmaceutical Chemistry, Institute of Pharmacy, Nirma University, Sarkhej-Gandhinagar Highway, Ahmedabad-382 481, Gujarat, India.*

[2]*Department of Pharmaceutical Chemistry, L.M. College of Pharmacy, Navrangpura, Ahmedabad-380 009, Gujarat, India.*

ABSTRACT: In continuation of our efforts to develop a potent and selective peripheral H_1 receptor antagonist for the treatment of allergic rhinitis or urticaria, earlier, we reported potent H_1-receptor antagonistic activity in a series of N_1-(substituted)aryl-2-(substituted)-5,7-dimethyl pyrido[2,3-*d*]pyrimidin-4(3*H*)-one. Three-dimensional quantitative structure-activity relationship (3D-QSAR) studies were performed on H_1 receptor antagonists based on Comparative Molecular Field Analysis (CoMFA) method. Significant correlation coefficients, r^2 = 0.894 and q^2 = 0.491 were obtained and the generated model was externally validated using test sets with r^2 predicted 0.624. The CoMFA model can be used to design novel, potent and selective H_1 receptor antagonists prior to their synthesis.

KEYWORDS: Pyridopyrimidines; • H_1 receptor antagonist; • 3D-QSAR; • CoMFA; • Tripose.

Background

Histamine is a neurotransmitter released in a variety of allergic conditions such as seasonal rhinitis (hay fever), urticaria (rash), pruritis, and insect stings as well as a reaction to certain drugs such as penicillin or aspirin. Histamine mediates its activity by interaction at H_1 receptors. Agents that selectively block these receptors are therefore of benefit in histamine-related allergic responses. Although very effective, the first-generation antihistamines which appeared in clinical practice during the 1940s suffered from two major drawbacks. First, they were highly lipid soluble and readily penetrate the blood-brain barrier (BBB) so cause marked sedation and second their nonselectivity for peripheral H_1 receptors at the given doses, so cause anticholinergic adverse effects, resulting in performance or cognitive function impairment and therapy non-adherence[1-7].

The second and third-generation antihistamines known as the "nonsedating antihistamines" were developed to minimize these side effects. Chemical structures of these drugs often deviate from the basic structure of classical antihistamines but they fulfill specific lipophilicity criteria which prevent them to cross BBB. Their activity is very sensitive to the precise stereochemistry and specific molecular interactions between drug and receptor. In continuation of our efforts to develop novel third generation H_1-receptor antagonist, we designed, synthesized and screened a series of N_1-(substituted)aryl-2-(substituted)-5,7-dimethylpyrido[2,3-*d*]pyrimidin-4(3*H*)-one[8]. The structures of these compounds and their biological activities are listed in Table 1.

* *For correspondence:* Bhumika d. Patel,

Phone: +91 2717 141900-04; Fax: +91 2717 241916

E-mail: bhumika.patel@nirmauni.ac.in

Table 1 Molecular structures of pyridopyrimidine derivatives with their respective log pA_2 values

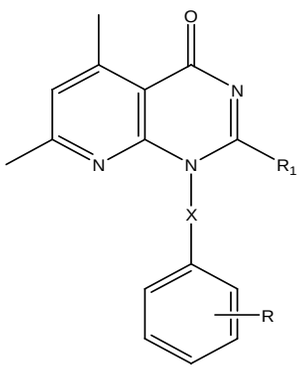

No.	X	R	R_1	log pA_2
1*	-	H	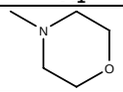	0.9148
2	CH_2	H	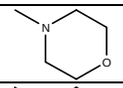	0.9375
3	-	m-CH_3	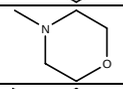	0.9079
4	-	p- CH_3	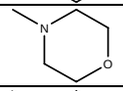	0.8779
5*	-	m-OCH_3	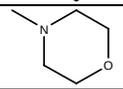	0.9498
6	-	p-OCH_3	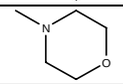	0.9164
7	-	p-F	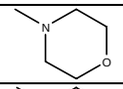	0.9434
8	-	m-Cl	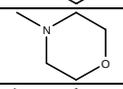	0.9493
9	-	p-Cl	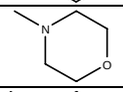	0.9253
10	-	p-Br	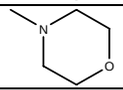	0.9703
11	-	2,3- di(CH_3)	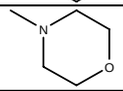	0.941
12*	-	2,4- di(CH_3)	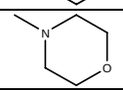	0.939
13*	-	H	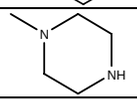	0.875
14	CH_2	H	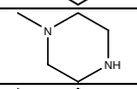	0.8633
15	-	m- CH_3	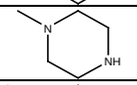	0.9493
16*	-	p-CH_3	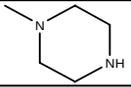	0.941
17	-	m-OCH_3	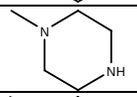	0.9508
18*	-	p-OCH_3	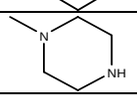	0.939
19*	-	p-F	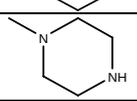	0.9532
20	-	m-Cl	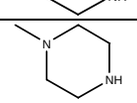	0.9405

Table 1 *Contd...*

No.	X	R	R_1	log pA_2
21	-	p-Cl	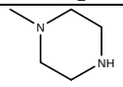	0.94
22*	-	p-Br	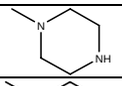	0.9774
23	-	2,3- di(CH_3)	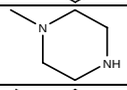	0.9079
24*	-	2,4- di(CH_3)	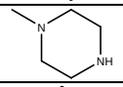	0.8774
25	-	H	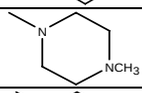	0.918
26	CH_2	H	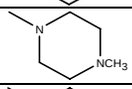	0.9159
27*	-	m- CH_3	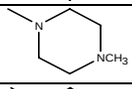	0.9232
28	-	p- CH_3	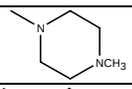	0.9132
29*	-	m-OCH_3	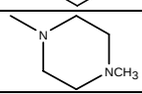	0.9756
30	-	p-OCH_3	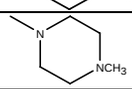	0.9426
31*	-	p-F	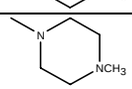	0.9604
32	-	m-Cl	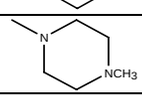	0.9561
33	-	p-Cl	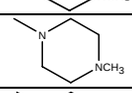	0.9365
34	-	p-Br	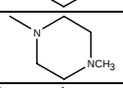	0.9777
35*	-	2,3- di(CH_3)	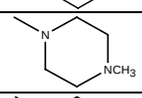	0.9164
36*	-	2,4- di(CH_3)	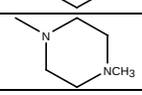	0.9294
37	-	H	-$N(CH_3)_2$	0.8677
38*	CH_2	H	-$N(CH_3)_2$	0.9063
39	-	m- CH_3	-$N(CH_3)_2$	0.9077
40*	-	p- CH_3	-$N(CH_3)_2$	0.8776
41	-	m-OCH_3	-$N(CH_3)_2$	0.9263
42	-	p-OCH_3	-$N(CH_3)_2$	0.9253
43*	-	p-F	-$N(CH_3)_2$	0.9518
44*	-	m-Cl	-$N(CH_3)_2$	0.8621
45*	-	p-Cl	-$N(CH_3)_2$	0.9222
46	-	p-Br	-$N(CH_3)_2$	0.9561
47	-	2,3- di(CH_3)	-$N(CH_3)_2$	0.9395
48	-	2,4- di(CH_3)	-$N(CH_3)_2$	0.9289
49*	-	H	-$N(C_2H_5)_2$	0.877
50	CH_2	H	-$N(C_2H_5)_2$	0.9079
51	-	m- CH_3	-$N(C_2H_5)_2$	0.9132

Table 1 *Contd...*

No.	X	R	R_1	log pA_2
52*	-	p- CH_3	$-N(C_2H_5)_2$	0.939
53	-	m-OCH_3	$-N(C_2H_5)_2$	0.9459
54	-	p-OCH_3	$-N(C_2H_5)_2$	0.9283
55*	-	p-F	$-N(C_2H_5)_2$	0.9508
56	-	m-Cl	$-N(C_2H_5)_2$	0.9561
57*	-	p-Cl	$-N(C_2H_5)_2$	0.9148
58	-	p-Br	$-N(C_2H_5)_2$	0.9774
59*	-	2,3- di(CH_3)	$-N(C_2H_5)_2$	0.94
60	-	2,4- di(CH_3)	$-N(C_2H_5)_2$	0.9395
61*	-	H	$-NH(CH_2)_2N(C_2H_5)_2$	0.9763
62	CH_2	H	$-NH(CH_2)_2N(C_2H_5)_2$	0.9881
63	-	m- CH_3	$-NH(CH_2)_2N(C_2H_5)_2$	0.9339
64*	-	p- CH_3	$-NH(CH_2)_2N(C_2H_5)_2$	0.9057
65	-	m-OCH_3	$-NH(CH_2)_2N(C_2H_5)_2$	0.9289
66	-	p-OCH_3	$-NH(CH_2)_2N(C_2H_5)_2$	0.9561
67	-	p-F	$-NH(CH_2)_2N(C_2H_5)_2$	0.9854
68	-	m-Cl	$-NH(CH_2)_2N(C_2H_5)_2$	0.94
69	-	p-Cl	$-NH(CH_2)_2N(C_2H_5)_2$	0.9765
70	-	p-Br	$-NH(CH_2)_2N(C_2H_5)_2$	0.9885
71*	-	2,3- di(CH_3)	$-NH(CH_2)_2N(C_2H_5)_2$	0.9405
72	-	2,4- di(CH_3)	$-NH(CH_2)_2N(C_2H_5)_2$	0.9415
73	-	H	$-NH(CH_2)_3N(C_2H_5)_2$	0.8859
74	CH_2	H	$-NH(CH_2)_3N(C_2H_5)_2$	0.9164
75	-	m- CH_3	$-NH(CH_2)_3N(C_2H_5)_2$	0.9779
76*	-	p- CH_3	$-NH(CH_2)_3N(C_2H_5)_2$	0.9289
77	-	m-OCH_3	$-NH(CH_2)_3N(C_2H_5)_2$	0.9434
78	-	p-OCH_3	$-NH(CH_2)_3N(C_2H_5)_2$	0.9276
79*	-	p-F	$-NH(CH_2)_3N(C_2H_5)_2$	0.9786
80	-	m-Cl	$-NH(CH_2)_3N(C_2H_5)_2$	0.9508
81*	-	p-Cl	$-NH(CH_2)_3N(C_2H_5)_2$	0.9774
82	-	p-Br	$-NH(CH_2)_3N(C_2H_5)_2$	0.989
83	-	2,3- di(CH_3)	$-NH(CH_2)_3N(C_2H_5)_2$	0.9552
84	-	2,4- di(CH_3)	$-NH(CH_2)_3N(C_2H_5)_2$	0.938
85	-	H	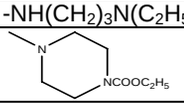	0.9175
86*	CH_2	H	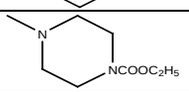	0.9477
87	-	m- CH_3	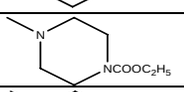	0.9772
88	-	p- CH_3	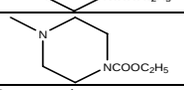	0.9115
89	-	m-OCH_3	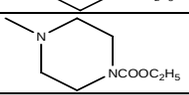	0.9484
90*	-	p-OCH_3	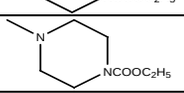	0.938
91*	-	p-F	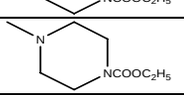	0.9863
92	-	m-Cl	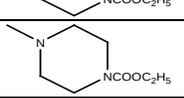	0.9647
93*	-	p-Cl	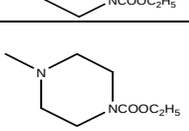	0.9175

Table 1 *Contd...*

No.	X	R	R_1	log pA_2
94	-	p-Br	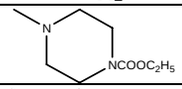	0.9885
95	-	2,3- di(CH_3)	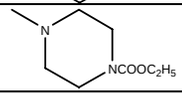	0.9385
96*	-	2,4- di(CH_3)	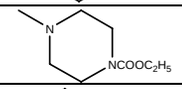	0.9329
97*	-	H	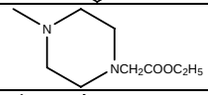	0.8764
98	CH_2	H	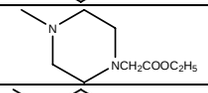	0.9489
99	-	m- CH_3	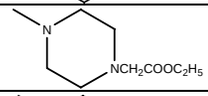	0.9175
100*	-	p- CH_3	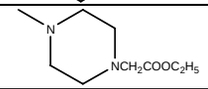	0.9566
101	-	m-OCH_3	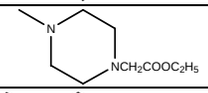	0.9277
102	-	p-OCH_3	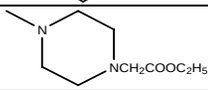	0.9656
103	-	p-F	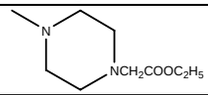	0.9604
104*	-	m-Cl	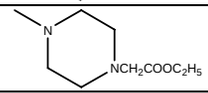	0.9434
105	-	p-Cl	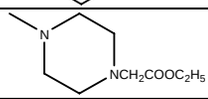	0.9599
106	-	p-Br	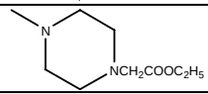	0.9758
107	-	2,3- di(CH_3)	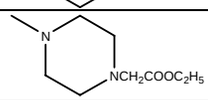	0.9375
108	-	2,4- di(CH_3)	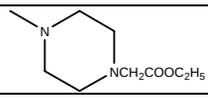	0.9319

* Test set compounds

Some of the compounds were found to be more potent than standard drug cetrizine with very low sedative potential and were found to be devoid of anticholinergic side-effects. In order to obtain the most potent and safe molecule in the series, for further lead modification and lead optimization 3D-QSAR study was performed using Comparative molecular field analysis (CoMFA) which may serve to provide useful information on the structural requirements for the antagonist action in terms of contour maps to aid the design of H_1-receptor antagonists prior to synthesis.

Results and Discussion

CoMFA technique was used in order to derive stable 3D QSAR model for 108 N_1-(substituted)aryl-2-(substituted)-5,7- dimethylpyrido [2,3-*d*] pyrimidin- 4 (3*H*)-one H_1 inhibitors. In order to examine the predictive ability and robustness of the CoMFA model, the whole data set of 108 compounds (Table 1) was divided into two parts- the training set consists of 70 compounds and the test set, selected randomly, comprised of 38 compounds. The pA_2 values of the molecules were converted into corresponding

logarithmic values and used as dependent variables. The produced QSAR model was further validated by performing a test set prediction using 38 molecules.

Table 1 lists all structures used in the training and test sets and their logarithmic pA_2 values. Among the used molecules for the QSAR study, the highly bioactive compound 94 was selected as a template molecule. The selected atoms of the template which are common in all studied compounds for the superimposition during the alignment were N1, C2, N3, C4, C5, C6 and N7 as shown in Fig. 1. Fig. 2 illustrates the superimposition of all the molecules.

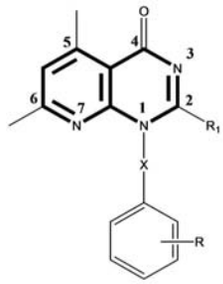

Fig. 1 Atom definition of pyridopyrimidine derivatives used for 3D-QSAR study

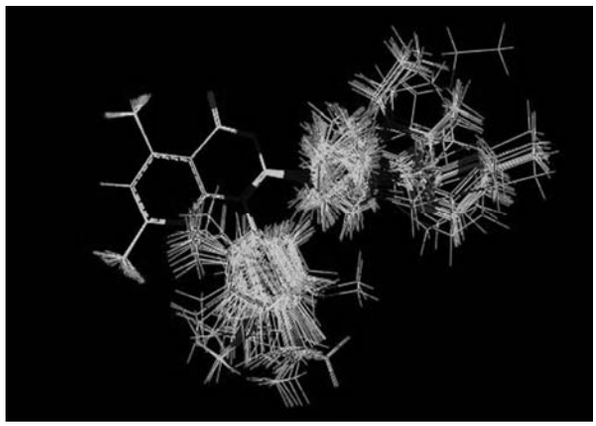

Fig. 2 Superimposition of pyridopyrimidine derivatives (training and test set)

The statistics of the final CoMFA model obtained from the PLS analysis, listed in Table 2. The developed CoMFA model gave a significant cross validated regression value of 0.491 with a standard error of prediction of 0.127. This partial least squares analysis suggested that the number of components to use in the non-cross validated regression model was eight. The resulting non-cross validated linear regression model gave a value of 0.894 and a standard error of estimate of 0.008. The relative contributions of the CoMFA variables to the model were also listed. These values constitute useful information to better understand to what extent the various steric and electrostatic regions can influence the binding of the ligand to H_1 receptor. The fact that the electrostatic contribution is only slightly higher than the steric one (60% *vs* 40%, respectively) means that the antagonistic activities of compounds for H_1 receptor are highly dependent on the electron density and molecular charges of the ligand.

Table 2 Statistical results for the best CoMFA model obtained for Pyridopyrimidine derivatives

q^2	0.491
SEP	0.127
n	8
r^2	0.894
SEE	0.008
F value (n1=8, n2=61)	64.306
Steric contribution	0.400
Electrostatic contribution	0.600
r^2 predicted	0.624

q2 : LOO cross-validated correlation coefficient;
SEP : Standard error of prediction;
r2 : non-cross-validated correlation coefficient;
n : number of components used in the PLS analysis;
SEE : standard error estimate;
F-value : F-statistic for the analysis.

The predictive ability of the model was determined from the test set of 38 compounds that were not included in the training set. These molecules were aligned in the same way as those in the training set and their activities were predicted by PLS analysis. Table 3 summarizes the predicted results obtained from the CoMFA model for training and test set. The plots of predicted versus actual activity for the training and test set inhibitors are shown in Fig. 3. By comparison of the experimentally observed and theoretically predicted log pA_2 values of a series of pyridopyrimidine derivatives, it can be seen that CoMFA model performed well in the prediction of the activities of the test inhibitors. In almost all the cases, the predicted values were close to the observed log pA_2 values, deviating by less than small logarithm unit.

Table 3 Experimental versus predicted activities (log pA2), with residual (s), for the pyridopyrimidine derivatives of the training and test set.

Compound No.	Experimental log pA_2	Predicted log pA_2	Residual
1*	0.9148	0.905	0.0098
2	0.9375	0.927	0.0105
3	0.9079	0.897	0.0109
4	0.8779	0.907	-0.0291
5*	0.9498	0.955	-0.0052

Table 1 *Contd...*

Compound No.	Experimental log pA_2	Predicted log pA_2	Residual
6	0.9164	0.925	-0.0086
7	0.9434	0.931	0.0124
8	0.9493	0.943	0.0063
9	0.9253	0.914	0.0113
10	0.9703	0.973	-0.0027
11	0.941	0.939	0.002
12*	0.939	0.907	0.032
13*	0.875	0.913	-0.038
14	0.8633	0.913	-0.0497
15	0.9493	0.935	0.0143
16*	0.941	0.918	0.023
17	0.9508	0.956	-0.0052
18*	0.939	0.935	0.004
19*	0.9532	0.918	0.0352
20	0.9405	0.941	-0.0005
21	0.94	0.951	-0.011
22*	0.9774	0.953	0.0244
23	0.9079	0.921	-0.0131
24*	0.8774	0.898	-0.0206
25	0.918	0.923	-0.005
26	0.9159	0.904	0.0119
27*	0.9232	0.91	0.0132
28	0.9132	0.924	-0.0108
29*	0.9756	0.952	0.0236
30	0.9426	0.941	0.0016
31*	0.9604	0.933	0.0274
32	0.9561	0.95	0.0061
33	0.9365	0.938	-0.0015
34	0.9777	0.977	0.0007
35*	0.9164	0.949	-0.0326
36*	0.9294	0.924	0.0054
37	0.8677	0.897	-0.0293
38*	0.9063	0.906	0.0003
39	0.9077	0.894	0.0137
40*	0.9776	0.901	0.0766
41	0.9263	0.926	0.0003
42	0.9253	0.927	-0.0017
43*	0.9518	0.908	0.0438
44*	0.8621	0.892	-0.0299
45*	0.9222	0.918	0.0042
46	0.9561	0.953	0.0031
47	0.9395	0.939	0.0005
48	0.9289	0.919	0.0099
49*	0.877	0.918	-0.041
50	0.9079	0.91	-0.0021
51	0.9132	0.912	0.0012
52*	0.939	0.922	0.017
53	0.9459	0.942	0.0039
54	0.9283	0.938	-0.0097
55*	0.9508	0.926	0.0248
56	0.9561	0.949	0.0071
57*	0.9148	0.947	-0.0322
58	0.9774	0.968	0.0094
59*	0.94	0.962	-0.022
60	0.9395	0.946	-0.0065
61*	0.9763	0.96	0.0163
62	0.9881	0.99	-0.0019
63	0.9339	0.939	-0.0051
64*	0.9057	0.889	0.0167
65	0.9289	0.934	-0.0051
66	0.9561	0.959	-0.0029
67	0.9854	0.978	0.0074

Table 1 *Contd...*

Compound No.	Experimental log pA_2	Predicted log pA_2	Residual
68	0.94	0.949	-0.009
69	0.9765	0.98	-0.0035
70	0.9885	0.993	-0.0045
71*	0.9405	0.95	-0.0095
72	0.9415	0.953	-0.0115
73	0.8859	0.928	-0.0421
74	0.9164	0.927	-0.0106
75	0.9779	0.966	0.0119
76*	0.9289	0.931	-0.0021
77	0.9434	0.946	-0.0026
78	0.9276	0.943	-0.0154
79*	0.9786	0.95	0.0286
80	0.9508	0.942	0.0088
81*	0.9774	0.978	-0.0006
82	0.989	0.974	0.015
83	0.9552	0.941	0.0142
84	0.938	0.927	0.011
85	0.9175	0.92	-0.0025
86*	0.9477	0.934	0.0137
87	0.9772	0.966	0.0112
88	0.9115	0.927	-0.0155
89	0.9484	0.961	-0.0126
90*	0.938	0.961	-0.023
91*	0.9863	0.941	0.0453
92	0.9647	0.959	0.0057
93*	0.9175	0.97	-0.0525
94	0.9885	0.979	0.0095
95	0.9385	0.94	-0.0015
96*	0.9329	0.944	-0.0111
97*	0.8764	0.929	-0.0526
98	0.9489	0.952	-0.0031
99	0.9175	0.908	0.0095
100*	0.9566	0.933	0.0236
101	0.9277	0.929	-0.0013
102	0.9656	0.98	-0.0144
103	0.9604	0.953	0.0074
104*	0.9434	0.95	-0.0066
105	0.9599	0.951	0.0089
106	0.9758	0.987	-0.0112
107	0.9375	0.943	-0.0055
108	0.9319	0.936	-0.0041

* Test set compounds

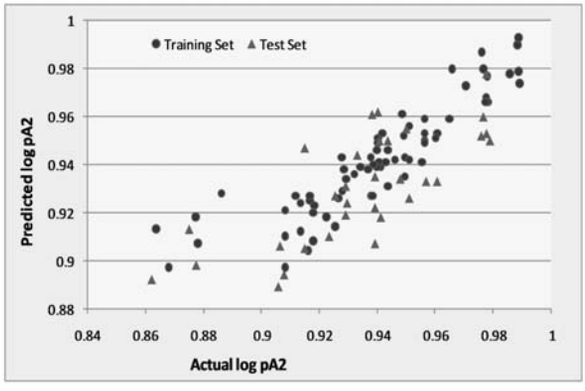

Fig. 3 CoMFA predicted versus actual log pA_2 values for the training and test set. Correlation coefficient (r^2) = 0. 894 for training set and 0.624 for test set.

The predictive correlation coefficient (r^2 pred) is defined as $r^2_{pred} = (SD - PRESS)/SD$ Where SD is the sum of squared deviations between the biological activities of the test set and mean activity of the training set molecules and PRESS is the sum of squared deviation between predicted and actual activity values for every molecule in the test set. The r^2 pred obtained was 0.624 for the CoMFA model (Table 2) which indicates good external predictive power of the model. All results including statistical data from this predictive validation analysis further confirmed the robustness of the obtained model in terms of their predictive ability.

From the validated CoMFA model, it is possible to identify regions of space around the molecules where changes with altering substitution would lead to an increase or a decrease biological activity. This was achieved by using a CoMFA

contour map for the model, as shown in Fig. 4 and 5. Fig. 4 shows the steric contour map for the CoMFA model with one of the highly active inhibitor 94 (log pA_2 = 0.9885) as a reference. The steric field defined by the green colored contours represents regions of high steric tolerance, while yellow colored contours represent regions of unfavorable steric effect. Fig. 5 shows the electrostatic contour map where the blue colored contours represent the regions where positively charged groups enhance the activity and red colored contours where the negatively charged groups enhance the activity.

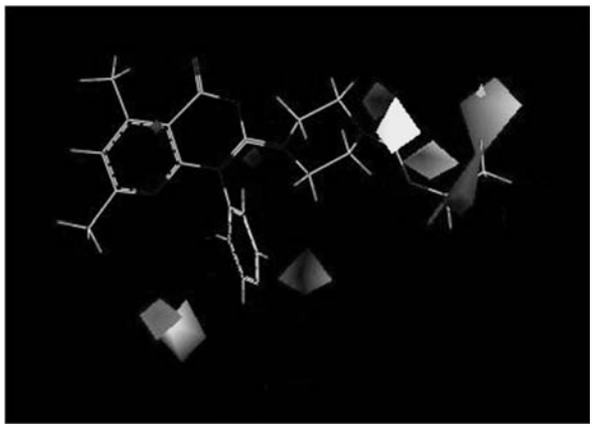

Fig. 4 Standard coefficient steric contour map of final CoMFA analysis. Green contours (80% contribution) refer to sterically favored regions and yellow counters (20% contribution) are sterically unfavored.

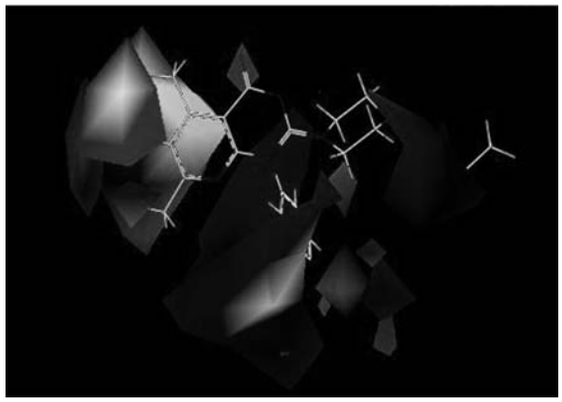

Fig. 5 Standard coefficient electrostatic contour map of final CoMFA analysis. Blue contours (80% contribution) refer to regions where positively charged substituents are favored; red contours (20% contribution) indicate regions where negatively charged substituents are favored.

The CoMFA steric map displays green colored contours bordering the terminal end of R_1 substituent while yellow colored contours are mapped on the carbonyl group of R_1 (bulky group disfavored) in the reference molecule. CoMFA electrostatic map displays blue colored contours around the carbonyl group of R_1 (negative charged groups disfavored) explaining the decreased activity. On the other side, green contours around R_1 indicate that length and bulk of tail of the side chain play a critical role in determining the biological activity as long chain is favorable for the activity with electropositive atoms. In the case of highly active compounds **70** (R_1 = -$NH(CH_2)_2N(C_2H_5)_2$, log pA_2= 0.9885) and **82** (R_1 = -$NH(CH_2)_3N(C_2H_5)_2$, log pA_2= 0.989), long and bulky substituent as R_1 without any carbonyl function resulted in good activity in comparison to other molecules such as compound **14** (R_1 = piperazine ring, log pA_2= 0.8633) and **37,44** (R_1 = N.N-dimethyl, log pA_2= 0.8677 and 0.8621 respectively).

Green colored contours at the *para* position of the aryl ring indicate that bulky substitutions favor the activity. In every series, bulky halogens at *para* position (Compound **10, 22** and **70**) gave higher activity compared to smaller –CH_3 or -H groups (Compound **4 ,14** and **37**).

The CoMFA electrostatic contour map displays big zones around the whole 5,7-dimethylpyrido[2,3-*d*]pyrimidin ring. The blue contour around the aryl ring indicates that electropositive groups at any positions of phenyl ring increase the activity. The *para* position where a small red contour supports the conclusion that electronegative halogens increase the activity.

Red contour around the 5-methyl group of the 5,7-dimethylpyrido[2,3-*d*]pyrimidin ring suggests that instead of methyl more electronegative groups like halogens, oxygen, sulfur etc. can result in better activity profile.

Based on the results from CoMFA maps, it is possible to assume that the common pyridopyrimidine motif present in the derivatives is the most important part for the activity of this series. Furthermore, the length and bulk of R_1 side chain as well as electronic environment of aryl ring are the other influencing factors. The information obtained from the study provides a means for predicting the activity of this series of compounds for guiding further structural modifications and synthesis of potent H_1 antagonists.

Materials and Methods

Data Set and Molecular Modeling

The QSAR modeling analyses, calculations, and visualizations for CoMFA were performed using the SYBYL X1.2 package[9] running on windows based workstation. To obtain reliable results, the total 108 H_1 inhibitors of a N_1-(substituted)aryl-2-(substituted)-5,7-dimethylpyrido[2,3-*d*]pyrimidin-4(3*H*)-one series[8] were divided into two sets, the training set consisting of 70 compounds and the test set consisting of 38 compounds (Table 1). Selection of training set and test set molecules was done by considering the fact that thirty eight compounds of the test set cover approximately all range of

log pA_2 similar to that to that of training set. Thus, the test set was truly representative of the training set. The 3D structures of the compounds were created in MOL2 format using the sketcher module of the SYBYL program. Gasteiger-Huckel charges were calculated for all compounds and then energy minimization was done using the Tripos force field.

Alignment of Molecules

One of the most important parameters in CoMFA is the relative alignment of all the compounds to one another so that they have a comparable conformation and a similar orientation of phrmacophoric groups in space[10]. In this study, the most active compound 94 was used as a template for superimposition, assuming that its lowest-energy conformation represents the most probable bioactive conformation of the pyridopyrimidine analogs at the H_1 receptor. The minimized molecules were superimposed (Fig. 2) by the atom-fit method choosing the seven features numbered from 1 to 7 in 5,7-dimethylpyrido(2,3-*d*)pyrimidin-4(3*H*)-one fragment (Fig.1).

PLS Analysis

CoMFA is a popular 3D-QSAR technique which uses Partial least square (PLS) as the data analysis method. PLS is then used to derive an equation that correlates the biological activity with the different probes at various lattice points[11]. Default values provided in the Tripos CoMFA module were used with 2.0 Å grid spacing using a sp^3 carbon atom with a +1 point charge as a probe to explore the steric and electrostatic interactions at the lattice points in the grid. The default cut-off value was set at 30 kcal/mol. Leave-one-out cross-validated PLS analysis was performed to determine the optimal number of components by a minimum predictive sum of squares (PRESS) value and maximum q^2. The q^2 statistic is defined as $q^2 = 1 - \Sigma (Y_{pred}-Y_{actual})^2 / \Sigma(Y_{actual}-Y_{mean})^2$ where Y_{pred}, Y_{actual}, and Y_{mean} are the predicted, actual and mean values of the target property respectively. $\Sigma (Y_{pred}-Y_{actual})^2$ is the PRESS. Cross-validation of the dependent column and the CoMFA column was performed with 2.0 kcal/mol column filtering to minimize the influence of noisy columns and scaled by the CoMFA standard deviation. . The q^2 values obtained were considered significant at 0.3. The optimal number of components was used to generate the final Non-cross validation PLS model and the 3D-QSAR model was used to predict the target properties of the compounds in the testing set. Non-cross validated (r^2) values were determined for the models using linear regression analysis (with variances reported as the standard error of estimation, SEE.) which were considered significant when r^2 is greater than 0.7. The 3D graphical representation of the steric and electrostatic fields generated through CoMFA are shown with the relative contributions represented as a 3D coefficient map with favored 80% steric (green) and electrostatic (blue) effects and 20% disfavored steric (yellow) and electrostatic effects (red). Green colored areas of the map indicate where sterically bulky groups may enhance interaction affinity. Blue colored areas (80%) indicate regions where a more positively charged group will likely lead to increased binding affinity, while red areas indicate where a more negatively charged group will likely lead to increased binding (20%).

Conclusion

In present study, the 3D-QSAR model, CoMFA was applied to predict the Histamine H_1 receptor antagonist activity of a series of substituted pyridopyrimidine derivatives. The best model had satisfactory statistical results in terms of q^2 and r^2 values, and showed excellent predictivity of the test set, in the external validation, showing no outliers. Information obtained from CoMFA maps gave good insight about the influence of various structural features for the H_1 antagonist activity and may be considered as a powerful tool in designing and forecasting more efficacious analogs.

References

[1] Paton, D.M.; Webster, D.R. Clin. Pharmacokinet. 1985, 10(6), 477-497.

[2] Simons, F.E. J. Allergy Clin. Immunol. 1989, 84(6), 845-861.

[3] Rimmer, S.J.; Church, M.K. Clin. & Exp.Allergy. 1990, 20, 3-17.

[4] Estelle, F.; Simons, R. Clin &. Exp. Allergy. 1990, 20, 19- 24.

[5] Simons, R.; Estelle, F.; Simons, K.J. N. Engl. J. Med. 1994, 330(23), 1663-1669.

[6] Feinberg, S.M.; Malkiel, S.; Berstein, T.B.; Hargis, B.J. J. Pharmacol. Exp. Ther. 1950, 99(2), 195-201.

[7] Hong, Y.; Gerald, J.T.; Wilkinson, H.S.; Roger, P.B.; Stephen, A.W.; Chris, H.S. Tetrahedron Lett. 1997, 38(32), 5607-5610.

[8] Suhagia, B.N.; Chhabria, M.T.; Makwana, A.G. J. Enzyme Inhib. Med. Chem. 2006, 21(6), 681-691.

[9] Sybyl 6.9, Molecular Modelling Software. Tripos Associates Inc., St. Louis MO 63144**,** U.S.A.

[10] Cramer III, R.D.; Patterson, D.E.; Bunce, J.D. J. Am. Chem. Soc. 1988, 110(18), 5959-5967

[11] Clark, M.; Cramer III, R.D.; Jones, D.M.; Patterson, D.E.; Simeroth, P.E. Tetrahedron Comput. Method. 1980, 3(1), 47-59